

Journal of Visualized Experiments

Ultrahigh Resolution Mouse Optical Coherence Tomography to Aid Intraocular Injection in Retinal Gene Therapy Research --Manuscript Draft--

Article Type:	Methods Article - JoVE Produced Video
Manuscript Number:	JoVE55894R2
Full Title:	Ultrahigh Resolution Mouse Optical Coherence Tomography to Aid Intraocular Injection in Retinal Gene Therapy Research
Keywords:	Optical Coherence Tomography, Retinal Degeneration, Greenough Microscopy, Imaging, Injection, In-vivo, Microscope, Photoreceptors, Preclinical, Real-time, Retina, Sub-retinal
Corresponding Author:	Jack M. Sullivan, M.D., Ph.D. University at Buffalo - The State University of New York Buffalo, NY UNITED STATES
Corresponding Author's Institution:	University at Buffalo - The State University of New York
Corresponding Author E-Mail:	jackmsullivanmdphd@yahoo.com
First Author:	Mark C. Butler
Other Authors:	Mark C. Butler
Author Comments:	We are trying to revise Figure 5E with a better 3D graphics program and will provide a revised Fig. 5 when completed.
Additional Information:	
Question	Response
If this article needs to be "in-press" by a certain date, please indicate the date below and explain in your cover letter.	12-31-2017

TITLE:

Ultrahigh Resolution Mouse Optical Coherence Tomography to Aid Intraocular Injection in Retinal Gene Therapy Research

AUTHORS AND AFFILIATIONS:

Mark C. Butler^{1,2}, Jack M. Sullivan¹⁻⁷

¹Research Service, VA Western New York Healthcare System, Buffalo, NY

²Department of Ophthalmology, (Ross Eye Institute), Jacobs School of Medicine and Biomedical Sciences, University at Buffalo- State University of New York (SUNY), Buffalo, NY

³Pharmacology/Toxicology, and ⁴Physiology/Biophysics, ⁵Neuroscience Program, Jacobs School of Medicine and Biomedical Sciences, University at Buffalo- SUNY, Buffalo, NY

⁶The RNA Institute, University at Albany- SUNY

⁷The SUNY Eye Institute

EMAIL ADDRESSES:

Jack M. Sullivan (js354@buffalo.edu)

Mark C. Butler (mcbutler@buffalo.edu)

CORRESPONDING AUTHOR:

Jack M. Sullivan (js354@buffalo.edu)

KEYWORDS:

Optical Coherence Tomography, Retinal Degeneration, Greenough Stereo Microscopy, Imaging, Intraocular Injection, *In Vivo*, Microscope, Photoreceptors, Preclinical, Real-time, Retina, Sub-retinal.

SUMMARY:

Here we demonstrate a novel approach to using high resolution spectral-domain optical coherence tomography (HR-SD-OCT) to assist delivery of gene therapy agents into the subretinal space, assess its areal coverage, and characterize photoreceptor vitality.

ABSTRACT:

HR-SD-OCT is utilized to monitor the progression of photoreceptor degeneration in live mouse models, assess the delivery of therapeutic agents into the subretinal space, and to evaluate toxicity and efficacy *in vivo*. HR-SD-OCT uses near infrared light (800-880 nm) and has optics specifically designed for the unique optics of the mouse eye with sub-2-micron axial resolution. Transgenic mouse models of outer retinal (photoreceptor) degeneration and controls were imaged to assess the disease progression. Pulled glass microneedles were used to deliver sub retinal injections of adeno-associated virus (AAV) or nanoparticles (NP) *via* a trans-scleral and trans-choroidal approach. Careful positioning of the needle into the subretinal space was required prior to a calibrated pressure injection, which delivers fluid into the sub retinal space. Real time subretinal surgery was conducted on our retinal imaging system (RIS). HR-SD-OCT demonstrated progressive uniform retinal degeneration due to expression of a toxic

mutant human mutant rhodopsin (P347S) (*RHO*^{P347S}) transgene in mice. HR-SD-OCT allows rigorous quantification of all the retinal layers. Outer nuclear layer (ONL) thickness and photoreceptor outer segment length (OSL) measurements correlate with photoreceptor vitality, degeneration, or rescue. The RIS delivery system allows real-time visualization of subretinal injections in neonatal (~P10-14) or adult mice, and HR-SD-OCT immediately determines success of delivery and maps areal extent. HR-SD-OCT is a powerful tool that can evaluate the success of subretinal surgery in mice, in addition to measuring vitality of photoreceptors *in vivo*. HR-SD-OCT can also be used to identify uniform animal cohorts to evaluate the extent of retinal degeneration, toxicity, and therapeutic rescue in preclinical gene therapy research studies.

INTRODUCTION:

Researchers are developing gene therapies for a variety of retinal and retinal degenerative diseases with hopes of translating novel therapeutics into treatments for human disease¹⁻¹¹. Time domain or spectral domain optical coherence tomography (SD-OCT) has been used to investigate the aspects of outer retinal degeneration in specific mouse models of disease¹²⁻¹⁴. HR-SD-OCT has not, however, been extensively used in the context of optimizing evaluation of mouse models to determine the rate and spatial uniformity of retinal degeneration, or in the context of preclinical evaluation of gene based therapeutics, for example, to assess rescue, toxicity, or the spatial extent of vector delivery^{8,15,16}. Once a mouse model is fully characterized, the HR-SD-OCT data can serve as an informative and reliable resource to measure the impact of therapeutics to exert rescue or toxicity in mouse models of retinal degeneration¹⁷. Many groups are using subretinal injection as a method of vector delivery due to its efficiency at transducing photoreceptors and retinal pigment epithelium (RPE) cells. However, this remains a difficult method to master, given that it is typically done by free-hand surgery from the corneal surface, and is often fraught with cataracts, bleeding, and unintended retinal detachments occurring simply by manipulation of the posterior vitreous. Many groups still attempt subretinal injections blindly and deliver the virus using manual injections with relatively large diameter stainless steel needles (34G)^{8,17,18,19,20,21,22}, and a few uses optical coherence tomography (OCT) imaging to confirm proper delivery of vector to the retina^{8,17,20,22}. Some improvements in the method have recently been described using microscale needles driven by a micromanipulator²².

We present an integrated approach which aids in the positioning of the needle, and the injections are facilitated by a custom directed stereo ophthalmoscope designed in the lab specifically for visualizing inside the small eye of the mouse^{17,23}. The use of pulled glass micro needles in conjunction with the stereotaxic micromanipulator provide better control of needle placement with no surgical cut down required (*i.e.*, through conjunctivae and connective tissue) prior to injection. The use of the pressure regulated micro injector helps deliver consistent injection volumes, and the injection can be done with much greater stability, precision, and much slower than manual injections performed by a hand-held syringe, thereby decreasing the occurrence of bubble injection into the eye. The smaller needle helps prevent leakage following needle withdrawal because the path is self-sealing. To assess the extent of injection/delivery, many investigative groups rely on finding and assessing the areal extent of enhanced green fluorescence protein (EGFP) expression in the retina (expression construct delivered by the vector) at the experimental end point (euthanasia) to confirm successful injections^{11,19,20,24}. This

approach (not utilizing OCT) to verify surgical success wastes an enormous amount of resources in surgical procedural time and animals, since all animals with (unknown) surgical failures need to be maintained, followed with repetitive measures until euthanasia and eye harvest (when EGFP is measured). Confirmation of the location of injection in the retina can be improved using HR-SD-OCT to demonstrate that the injection is located between the correct layers of the retina (*i.e.* the subretinal space). HR-SD-OCT can also be used to immediately delineate unsuccessful attempts (surgical failures) to identify relevant variables in real surgical time to improve upon the approach. We found that HR-SD-OCT provides numerous advantages in preclinical gene therapy studies by allowing rapid quantitative evaluation of outer retinal degeneration, allowing identification/culling of study animals which do not meet experimental criteria (*e.g.*, incorrect subretinal injection), and to direct follow-up imaging to the region of the eye where vector was delivered (where preclinical effect is most likely) as well as control regions where vector was not delivered. Since its development, the use of SD-OCT has continued to be accepted and used by ophthalmology researchers and is now considered the standard of retinal imaging in retinal scientific studies in mouse or rodent models^{13, 25}. HR-SD-OCT and its software capabilities were utilized in unique integrated ways to further the goal of successful quantitative gene therapy in mouse models at every step in the process, including animal model selection, characterization of degeneration in chosen disease models, therapeutic delivery, mapping of vector delivery, and toxicity/efficacy evaluation. The use of HR-SD-OCT allows for more efficient drug discovery at every level of the process. Here we describe these approaches that are used in our RNA Drug Discovery program.

PROTOCOL:

Animal protocols were reviewed and approved by the Institutional Animal Care and Use Committees of the VA WNY HCS and the University at Buffalo-SUNY. Animals were used according to the stipulations of the Association for Research in Vision and Ophthalmology (ARVO) and the Declaration of Helsinki.

1. Mouse Models

1.1. Identify mouse models to be evaluated including controls.

Note: Imaging was performed for a C57BL/6(J), hC1/hC1//mWT/mWT, a partially humanized mouse retinal degeneration model homozygous for human mutant *RHO*^{P347S} hC1 alleles on the wild-type (WT) mouse *RHO*^{+/+} genotype^{26,27}, hC1 x BL/6(J), a partially humanized model with a single copy of the mutant human *RHO*^{P347S} hC1 allele on the WT mouse *RHO*^{+/+} genotype (hC1//mWT/mWT) (obtained by crossing hC1/hC1//mWT/mWT with C57BL/6(J) mice). The above autosomal dominant retinitis pigmentosa (adRP) models are on the C57BL/6(J) background. A mouse model that is homozygous for two copies of the human WT *RHO* gene on the mouse *RHO* knockout background was also used^{28,29}. This line is on the 129Sv background. When this line was crossed with a mouse *RHO* knockout on the 129Sv background, a single dose of human *RHO* occurs on the mouse *RHO* background.

1.2. Maintain the animals following the conditions pertinent to the experimental design.

Note: The animals were maintained in the Veterinary Medical Unit (VMU) at the VA WNY HCS. Mice were fed standard lab chow and grown under 12 h:12 h light: dark cycles with soft fluorescent overhead white lights with approximately 300 lux at cage level at approximately 72 °F.

2. Mouse Eye Gel

2.1. Prepare the optical gel used for retinal imaging³⁰ and surgical procedures.

2.2. Combine 2 mg/mL w/v high molecular weight (4×10^6 g/mol carbomer in sterile 1x Phosphate Buffered Saline (PBS).

2.3. Mix at room temperature until the gel forms a viscous optically transparent gel.

2.4. Transfer the gel into small sterile bottles and centrifuge in a swinging bucket tabletop centrifuge at 350 x g to remove trapped air bubbles.

2.5. Apply the gel directly to the cornea to create an interface between the mouse cornea and a premium cover glass (18 mm x 18 mm).

3. HR-SD-OCT Imaging

3.1. See the HR-SD-OCT device (**Figure 1**).

3.2. Weigh the animal to determine the proper dose of anesthetic. Then anesthetize the mouse using 25 µL/g of body weight of the Avertin solution and add the eye drops to dilate the pupils after the animal is immobilized.

3.3. Confirm that the animal is fully anesthetized by a toe pinch, and be certain the animal does not react.

3.4. Trim the whiskers and place the mouse onto the HR-SD-OCT sled.

3.5. Position the mouse's eye directly in front of the headpiece lens and manipulate the stage controls until the cornea and iris are located. Keep the cornea hydrated by applying artificial tears.

Note: The fine adjustment micromanipulators on the HR-SD-OCT sled are used to position the mouse such that the pupil aperture is centered and oriented. The optical headpiece is then advanced until the retina becomes visible and the animal is further adjusted to obtain the best possible image.

3.6. First, open the software program “Mouse” and click “patient/exam”. Second, click “add patient” and enter the pertinent information to identify the animal in the new patient window and “save and Exit”. Third, click “add exam” followed by “start exam”. Fourth, click “add custom scan” and select “rectangular volume”, choose OD or OS for the eye being imaged, then click “add exam”. Finally, start aiming the instrument and positioning the animal to obtain the region of interest. After finding the correct region, remove any excess fluid from the eye surface using a sterile cotton tipped applicator just prior to image acquisition in order to further enhance image quality, then click “start snapshot”, and if a good image is obtained, click “save scan”.

Note: Typical parameters for rectangular HR-SD-OCT images are 900 a-scans/b-scan and 90 b-scans/image. Acquired images are 1.4 mm x 1.4 mm. The region of the retina imaged depends on the specific experiment, but most images are centered on the optic nerve head (ONH).

4. Assessing the Presence, Rate, and Uniformity of Model Outer Retinal Degenerations

4.1. Outer Retinal Degeneration Model Evaluation by HR-SD-OCT

4.1.1. Obtain animals with a wide spectrum of ages for both the control and experimental subjects to assess the presence, rate, and uniformity of outer retinal degeneration.

4.1.2. Perform HR-SD-OCT imaging on multiple animals at each age from both cohorts (disease and normal). Use the method described in 3.1.6 to obtain the OCT images.

Note: Data can be collected from a large cohort of animals all at once, which have distributed birthdays spanning a wide period of time (1 year), or a small cohort of animal can be used to collect multiple images over a long period of time (1 year) to obtain similar results.

4.1.3. Open a recorded HR-SD-OCT rectangular volume image, and identify the first b-scan to be measured (ideally will include the ONH or other identifiable landmark) from the ensemble of images. Enlarge the image to fill the screen using the zoom feature in the software.

4.1.4. Open the desired number of calipers by right clicking on the image of the b-scan and then clicking on “Calipers” and finally clicking on as many calipers as desired (they are numbered 1 through 10). Ensure that the calipers show up in lower right corner of the image. Using the “Configure Caliper” feature, assign them all as “vertical” in the angle block column and turn on the “Display Caliper Location” to facilitate uniform placement across the retina and finally, click apply.

Note: The 1st caliper should be placed on the left side of the image when processing the oculus dexter (OD) right eye and the 1st Caliper should be placed on the right side of the image when processing the oculus sinister (OS) left eye images. This results in a nasal to temporal orientation of all the data for both the left and right eyes when plotting.

219 4.1.5. Using the computer mouse, move each caliper to the desired location (2.0 mm apart)
220 across the b-scan, being sure to place one caliper in the center of the optic nerve head, in b-
221 scan images that include it (set this caliper to zero). Then use the mouse to click and drag the
222 caliper to length to span the region of interest. Arbitrarily set calipers that do not overlay
223 measurable regions of the b-scan to maximum length, and ignore during the data analysis.

225 4.1.6. Measure the ONL thickness using the Caliper tools, by placing the top of the caliper at the
226 external limiting membrane (ELM) and the bottom of the caliper at the bottom of the outer
227 plexiform layer (OPL). Repeat this for each caliper across the retina at 0.2 mm increments. Save
228 the measurements.

229
230 4.1.7. After all calipers have been placed and adjusted to size, right click on the image and click
231 "Save Caliper Data".

232
233 4.1.8. Repeat measurements on subsequent b-scans (every 10th scan works well) from the same
234 rectangular volume OCT image spanning the entire retina from inferior to superior regions.
235 Calipers should remain open and at the same location in the X-axis. Adjust the length of the
236 calipers without moving them in the X-direction.

237
238 4.1.9. Open the save data files by clicking the small file icon next to the processed b-scan image
239 and click "Go to Data". Click "Date Modified" to arrange the files in order based on time saved,
240 and open all the files for each b-scan measured.

241
242 4.1.10. Compile the raw data from each b-scan into a single file in order from lowest to highest
243 based on frame number. Select the columns of data including "Caliper name", "Length", and
244 "Center X".

245
246 4.1.11. Ensure that the center X is the same for all b-scans measured for each rectangular
247 volume OCT image processed. Delete any data from calipers that were not used to record
248 measurements, and set the caliper located at the center of the optic nerve head to zero.

249
250 4.1.12. Plot the data for X vs. multiple Y data sets to get a 3D plot function to plot the overall
251 thickness of the ONL or another measured retinal layer.

252
253 4.1.13. Compare ONL measurements between control and experimental animals with
254 corresponding ages to determine the rate and uniformity of any potential retinal degeneration.

255
256 4.1.14. Repeat the process for OSL measurements using the same b-scan images. Follow the
257 same methodology used to measure the ONL, except placing the calipers between ELM and
258 Bruch's membrane (BM).

259
260 **Note:** An example of how to place the caliper is shown in Representative Results section (**Figure**
261 **3B**). This should be done on a zoomed in image to decrease error.

4.1.15. Repeat the data analysis for multiple animals for each birthday for both experimental and control cohorts.

4.2. Comprehensive measurement and 3D mapping of the ONL or OSL thickness using the software calipers tool

4.2.1. Review the post injection OCT images and make note of any identifiable landmarks, like the ONH or blood vessels in the retina. Then position the mouse to obtain a follow-up SD-OCT from the same region, and be sure to include the same identifiable landmarks.

Note: Ensure that the region of the retina imaged and involved in the retinal detachment is identified in the post injection SD-OCT images. Record a rectangular volume SD-OCT image and save it.

4.2.2. Process the recorded images as described above in steps 4.1.3. to 4.1.14. Save the caliper data and plot as described above.

Note: The resulting array of ONL measurements is used to create a 3D plot depicting the ONL thickness. The position of the calipers along the X-axis allow one to replot the graph placing the optic nerve at the origin (0) along the X-axis. The Y-axis is plotted using the b-scan number and the optic nerve is then used to define the starting point, which allows one to properly position the optic nerve at the origin on the Y-axis. Identifying the optic nerve in each data set allows follow-up images to be aligned reliably.

4.3. Mapping the extent of the injection site onto the fundus image

4.3.1. Perform post injection rectangular volume OCT to confirm the success of the injection. Follow the method described in 3.6.

4.3.2. Use the Caliper feature in the software to identify the inflection point at the border of the detached retina from a number of b-scans spanning the entire OCT image. Use the method to open calipers described in 4.1.4.

4.3.3. Record the fundus images with the mapped location of the OCT b-scan and corresponding caliper position on the fundus image, which corresponds to its location.

4.3.4. Compile all of the fundus images into a composite image, including the caliper positions, which results in a precise map of the injection site onto the fundus image (Example in Representative Results section, Figure 5A).

5. Intraocular Injections

Note: Details on use of the RIS are further elaborated in a recent study²³.

5.1. Preparing glass injection needles

5.1.1. Autoclave the capillary tubes with filaments in small batches, using the dry cycle.

5.2.2. Use a pipette puller and set-up a program that will produce a glass tip with the sharpest angle, and a diameter in the range of 2-5 μm .

Note: A sample 5 step program which produced effective needles on our pipette puller is shown in **Table 1**.

5.2.3. Store the pulled glass needles in a sterile pipette needle jar at room temperature.

5.3. Fill the injection needle with the desired solution for injection

5.3.1. Mount the needle into the needle holder, leaving approximately 5/8" protruding beyond the end of the holder.

Note: A distance less than 5/8" will make it difficult reach the injection solution to fill the needle, because the needle holder does not fit readily into the opening of 0.2 mL tubes. Also, having the needle protrude more than 5/8" results in significantly larger oscillation or precession of the tip, making real time imaging difficult since the tip leaves the focal plane or the field of view (FOV), while attempting to puncture the eye.

5.3.2. Prepare the injection solution in a sterile 0.2 mL tube. Add a 1:10 dilution of sterile fluorescein sulfate (10 mg/mL in 1x PBS) to the injection solution to obtain a final concentration of fluorescein at 1 mg/mL.

Note: The exact dye used is specific to the user and can be anything that is non-toxic and visible to the naked eye under white light illumination to help facilitate precise placement of the needle tip at the level of the RPE and subretinal space.

5.3.3. Visualize the needle through the stereo microscope while using the control knobs of the 3-axis micromanipulator to position the needle so that it is aligned with the center of the tube containing the injection solution to be used for filling the needle.

5.3.4. Carefully drive the needle tip into the 0.2 mL tube until the tip of the needle is submerged in the fluid. Draw up the desired volume of injection fluid (e.g. 1 μL) into the needle necessary for a single injection. Maintain the remaining solution in the tube placed in ice.

5.4 Preparing the animal for injection

Note: The RIS microscope is kept clean, and is a non-contact system. The heating plate is covered with a clean adsorbent pad and needles are autoclaved prior to being pulled. After they are pulled by a self-sterilizing heated metal strip, they are kept in a closed sterilized

chamber designed to hold pulled glass needles. The needles are only handled using gloved hands, and care is used to prevent touching the tip of the needle while mounting it into the holder. The injected solutions are prepared using sterile technique, and are tested for contamination by streaking a sample of the virus preparations onto LB agar plates and incubating them over night at 37 °C.

5.4.1. Weigh the animal (g) to determine the appropriate dose of anesthetic analgesic.

5.4.2. Administer anesthetic (2.5% solution of buffered 2,2,2-tribromoethyl alcohol (Avertin)) *via* intraperitoneal injection (IP).

5.4.3. Immediately apply anticholinergic drugs (*e.g.*, cyclopentylate) to both eyes to dilate the pupils.

5.4.4. Trim the animal's whiskers and number the animal using ear punch or other method.

5.4.5. Wash the eye and surrounding area with diluted betadine.

Note: Avoid getting any solution around the nose, as this can result in unintentional drowning.

5.4.6. Place the mouse on the heating pad, maintained at 39 °C, in the pre-molded modeler's clay mouse holder with the eye to be injected towards the needle.

5.4.7. Make sure the mouse is unresponsive using a pinch test of the hind foot.

5.5. Performing subretinal injection

5.5.1. Use a pair of sterile blunt iris forceps to gently induce proptosis of the globe by placing the tips of the forceps at 7 and 10 o'clock positions on the eye lids while pushing open and downward at the same time.

5.5.2. Use the forceps to coax the eyelids under the eye globe to keep it out of the socket during the injection process.

Note: Animals 10 to 14 days old will often hold the eye out of the socket more easily than older animals.

5.5.3. Direct the tip of the needle about 1-1.5 mm below the edge of the corneal limbus and carefully drive it into the eye through the conjunctiva until it creates a scleral depression as the needle penetrates into the tissue of the sclera, and allows manipulation of the eye.

5.5.4. Rotate the eye downward with the micromanipulator to visualize the scleral depression through the dilated pupil with the RIS stereo microscope.

395 5.5.5. Apply a drop of sterile eye gel or 1x PBS solution and cover with a sterile coverslip.

396
397 5.5.6. Focus on the scleral depression created by the tip of the needle (2-5 μm), and drive the
398 needle forward until a sharp peak of the retina forms at the injection site.

399
400 5.5.7. Rotate the needle using the holder until the tip bores through the sclera and the
401 fluorescein in the needle is visible under the retina in the immediate vicinity of the RPE cell
402 monolayer.

403
404 5.5.8. Drive the tip of the needle so it is tangential to the globe, and then activate the injection
405 pump with the foot pedal switch.

406
407 5.5.9. After the desired volume has been delivered (0.5-1 μL) to the subretinal space, withdraw
408 the needle and check if the bleb is stable and that fluid does not leak out of the injection site,
409 which is the first criteria of a successful injection.

410
411 **Note:** Maintaining a proper tip diameter (2-5 μm diameter) is critical to avoid leakage from
412 injection site.

413
414 5.5.10. Place the animal on the imaging platform of the OCT instrument. Follow the directions
415 for HR-SD OCT Imaging to record a rectangular volume image.

416
417 5.5.11. Confirm that the injected fluid is located in the subretinal space, and save the images for
418 determining the extent of the bleb.

419
420 5.5.12. Remove the animal from the holder and apply an ample amount of antibiotic ointment
421 to the injected eyes.

422
423 5.5.13. Place the animal onto a heating pad until it completely recovers, then place it back into
424 the original cage where it came from.

425
426 **Note:** Our animals are usually injected prior to weaning, therefore the animals need to be
427 returned to the cage with the mother.

428 429 5.6. Mapping the extent of the subretinal bleb using OCT instrument software tools.

430
431 5.6.1. Obtain a rectangular volume OCT image, using methods described earlier, of the bleb and
432 position it to include a recognizable landmark within the eye such as the ONH.

433
434 **Note:** Recording 90 b-scans works well for mapping the bleb, but could be used depending
435 upon the desired resolution.

436
437 5.6.2. Add a single caliper to the figure and place it at the inflection point where the retina
438 detaches from the RPE and choroid.

Note: The software automatically maps a corresponding point to a line onto the fundus image representing the caliper and the b-scan being evaluated.

5.6.3. Capture the screen following placement of the calipers, and compile the images to effectively map the border of the injection bleb onto the fundus image, which precisely maps the injection site. Save the compiled image for reference to help in locating the regions of interest during follow-up imaging.

Note: Alternatively, the caliper data can be saved, compiled, and plotted using a similar method for plotting 3D data sets of ONL thickness.

5.7. Intravitreal Injection

5.7.1. Place the tip of the needle using a similar surgical approach as sub retinal injection, except that the needle is driven entirely through the sclera at the *pars plana* about 0.25 mm behind the corneal limbus and into the vitreous.

5.7.2. Following needle placement, apply the injection pulse with the foot pedal.

Note: A rapid diffusion of the fluorescein dye throughout the vitreous of the eyecup is observed, filling the dilated pupil aperture with fluorescence.

REPRESENTATIVE RESULTS:

Assessing the Presence, Rate and Uniformity of Model Outer Retinal Degeneration

Measurements of the ONL were recorded from the OPL to the ELM, defining the limits of the ONL using the caliper tool provided in the instrument software. The goal was to map the progression of outer retinal degeneration in a partially humanized adRP mouse model. Comparable images from a control C57BL/6(J) mouse and an hC1/hC1//mWT/mWT mouse model, expressing two copies of the mutant human rod opsin (*RHO*^{P347S}) genes, were shown to exhibit both the control retinal findings and those of a severe and rapidly progressive retinal degenerative condition. The 3-week-old adRP (hC1 x BL/6(J)) animal, having only a single copy of the mutant human *RHO*^{P347S} gene and two copies of the mouse WT *RHO* genes, had near normal ONL thickness. However, the follow-up HR-SD-OCT scans at 10 and 37 weeks demonstrated temporally progressive and spatially uniform retinal degeneration that resulted in approximately 60% loss of photoreceptors recognized as ONL thinning over this time frame. In the hC1 x BL/6(J) adRP model, the retinal degeneration has an approximate time constant (1/e) of 13 weeks. Homozygous hC1 animals, with two doses of the toxic mutant human transgene on the mouse WT *RHO* background, suffer a much more rapid degeneration as demonstrated by extensive retinal thinning and the essentially complete loss of all the photoreceptors by 3 weeks of age (**Figure 2**).

The ONL measure is only one component of outer retinal normality as an index of photoreceptor vitality. The OSL of the photoreceptors and the inner segment/outer segment (IS/OS) line or

ellipsoid line provide evidence in support of both photoreceptor vitality and function. Comparisons in animals which have been bred to contain either one (N129R- x 129R-) or two (2HRho 1T1T) copies (doses) of the human WT *RHO* genes on the mouse WT *RHO* knockout background were measured for outer retina thickness. A statistically significant increase of ~8 μ m in the ONL was observed in mice with two copies of the human WT *RHO* gene compared to mice with only one copy of the human gene. A statistically significant increase of ~5 μ m in the OSL was observed in mice with two vs. one copy of the human WT *RHO* gene on the mouse WT *RHO* knockout background. An example of how ONL and OSL measurements were made is shown in **Figure 3**. The high resolution of the images captured with the HR-SD-OCT system allow accurate measurements of the ONL or OSL allowing discrimination of small differences with solid statistical reliability in the humanized WT *RHO* mouse models.

Range of Surgical Outcomes Detailed by OCT when Attempting Subretinal Injection

HR-SD-OCT evaluation of attempted subretinal injections yielded a variety of outcomes. First, the most common experience was confirmation that the injected fluid was successfully delivered within the sub-retinal space. The opening of the implicit subretinal space (which closes during development) created a bleb that could be clearly visualized both in the *en face* view of the HR-SD-OCT and in the b-scan images. The hypo-reflective fluid was bordered by the neural retina above, and the hyper-reflective RPE cell layer still opposed to BM, below (**Figure 4**). The extent of the subretinal injection could be determined if the animal was imaged by HR-SD-OCT immediately after injection (see below). Second, the injection could occur in the choroidal space (beneath BM) rather than into the subretinal space. This resulted in a hyper-reflective layer (RPE) bounding the dome of the fluid-displaced region of the retina, and no hyper-reflectivity at the posterior limits of the eye in the OCT b-scans. Third, another potential result that could occur while attempting subretinal injection was a retinal schisis (splitting) at the nerve fiber layer. This result yielded a normal outer retina anatomy, but the inner layer of the retina encapsulated the bleb, which may or may not have invaded the vitreous. In principle, such a schisis pattern could occur with injection anywhere within the laminations of the neural retina proper, but we have only seen nerve fiber layer schisis to date. Fourth, an intravitreal injection may also occur, which has no impact on the OCT. All of these failures result from the initial misplacement of the tip of the glass needle, or perhaps some small motion of the needle during injection, due to the pressure head of the switched flow injection device.

Characterizing the Location of Subretinal Injection

A critical factor in determining efficacy or toxicity of candidate therapies is the ability to compare retinal regions that have received vector vs those that have not. We directed significant efforts into developing a means to mark the region of the retina involved in the subretinal injections so that during follow-up examinations, we could identify the areal extent of the retina where therapies were applied, and hence where transduction was feasible. Gold NPs allowed a high level of confidence in identifying regions of the retina which were or were not injected. However, the specific particles or their formulation appeared to be toxic and resulted in a severe localized retinal degeneration at the site of subretinal injection by 24 hours post injection (data not shown). Therefore, we developed an alternative method of mapping the injection site directly from the HR-SD-OCT imaging data. A method for precisely identifying the injection site borders

was developed using the measurement tools (calipers) in the software package of the instrument (**Figure 5**). We could identify the edge of the bleb precisely by examining the individual b-scans (from inferior to superior retina) used to create the fundus image. When placing a caliper at the point where the bleb intersects the attached retina, the position of the caliper is automatically mapped onto the corresponding b-scan of the *en face* fundus image at the precise position along the x-axis where the caliper was placed on the b-scan. Repeating this process allows one to trace the edge of the bleb onto an *en face* fundus image. The alignment process requires that similar regions of the retina are imaged every time, relative to the constant optic nerve head, and the images may need to be rotated to align the retinal blood vessels from the multiple images prior to data segregation. Following the alignment process of the post injection image and subsequent follow-up images, the injection region was superimposed over the data point grid to identify the position of the measurements within the region involved in the retinal detachment. This data could be plotted as a surface map, which provided a visual tool to identify data points inclusive of the injection site relative to regions outside of the injection site.

Mapping the ONL Thickness in 3D

Finally, we record measurements of the ONL, OSL, or other retinal layers from across the entire imaged region of the retina, and then plot the data using a surface plot (**Figure 5**). Superimposing the border map of the injection site allows the segregation of the two data sets, including the injected region and the region which was not detached during the injection process. Further processing and data analysis could then be performed on these two data sets to test hypotheses that specific therapeutic agents can rescue retinal degeneration or induce toxicity. This approach potentially allows for experimental and control data to be collected from a single eye, comparing injected vs non-injected regions of the same eye.

FIGURES AND TABLES:

Figure 1: UHR-SD-OCT Device. The HR-SD-OCT device used is shown. The instrument rack (**A**) contains the computer monitor (**a**), the keyboard and mouse (**b**), the probe interface box (**c**), the OCT engine (**d**), the computer (**e**), the control device for the super luminescent emitting diodes (infrared) (**f**), and the uninterruptible power supply (**g**). The optical bench (**B**) contains the imaging probe optical head (for mouse retina) (**h**), the multi-axis (linear and rotational) manipulator (**i**), and a mouse subject (**j**).

Figure 2: Progressive Outer Retinal Degeneration in partially humanized adRP model as measured by HR-SD-OCT. (**A**) HR-SD-OCT images of the retina were obtained for the adRP model (hC1 x BL/6 (J)) at different ages, the C57BL/6(J) control at 14 weeks, and the homozygous hC1 mutant line at 3 weeks. The outer retina had a normal appearance at 3 weeks in the adRP model, but there was evidence of progressive ONL thinning and disorganization at and beyond 10 weeks of age. By 37 weeks, the (hC1 x BL/6(J)) demonstrated extensive outer retinal degeneration. All OCT scans were in vicinity of optic nerve. (**B**) The ONL thickness (in mm) along the horizontal axis through the optic nerve was plotted for control (C57BL/6(J)), hC1, and adRP animals of differing ages. There was progressive loss of ONL thickness in the partially humanized adRP model. ONL

loss was greater than 60% by 37 weeks of age. Error bars = standard error of the mean. Red scale bar = 200 μ m and all the images are the same scale.

Figure 3: Quantitative measures of Outer Nuclear Layer and Outer segment length using HR-SD-OCT. (A) Mouse lines used to demonstrate ONL and OSL measures. Representative OCT images from 2HRho1T/1T (2 doses HRho) on mouse *RHO* knockout background) (Left panel) and N129R- x 129R- (one dose human *RHO* on mouse *RHO* knockout background) (Right panel). (B) An example of how calipers were placed to measure the ONL (red) and OSL (blue) is shown. (C) The data obtained from three animals of each line for ONL thickness was plotted in bar graph format showing comparison of 2HRho1T/1T line and N129R- x 129R- (Left panel). The 2HRho1T/1T line has ~8 μ m thicker ONL. To demonstrate differences in OSL, multiple measurements (seven) were made from one b-scan from each mouse line from the ELM to the BM as in B (blue line) in 9-week-old animals (Right panel). This demonstrated a ~5 μ m difference in the OSL between animals with 1 vs 2 copies of the HRho gene. Both ONL and the OSL measures were statistically significant, ONL p-value = 1.7e-5 and OSL p-value = 6.4e-5. Error bars = standard error of the mean. Red scale bar = 100 μ m both the b-scans in 3A have the same scale, 3B is zoomed to improve clarity of the retinal layers and to provide a qualitative demonstration of how the measurements were acquired.

Figure 4: Types of intraocular injections in mice identified by HR-SD-OCT. (A). A (hC1xBL/6(J)) mouse was injected with ~1 μ L of fluid via Inferonasal transcleral transchoroidal injection. The resulting retinal detachment is seen as the green lower right region of the *en face* image, creating a sharp border at the leading edge of the bleb on the right side of the image. The OCT fundus image of an injection site only exhibits subtle differences depending upon the position of the fluid filled cavity, because the image is a compilation of all the b-scans from the entire retinal thickness. In addition, the injection bleb changes the distance of the retinal surface from the OCT headpiece, producing an unfocused region at the injection site. (B) The OCT b-scan of a non-injected retina is demonstrated. The ONH is labeled. (C) A subretinal injection is demonstrated. The ONH is labeled, and arrows in the *en face* image (right panels) show the posterior border of the detachment. (D) A choroidal injection is demonstrated with a clear elevation (upward displacement) of the RPE layer (hyper-reflective curve) of the lower border of the retina (arrows) and significant loss of hyper-reflectivity of the RPE and choroid layers below the injected fluid. Compare arrows in the images (C vs. D). (E) A retinal schisis is demonstrated near the nerve fiber layer. Observe the very thin hyper-reflective membrane encapsulating the injected fluid, while the retina remains attached to the RPE. Subtle differences between the three different detachments can also be visualized in the *en face* images (C, D, and E). The subretinal detachment has a border which is difficult to visualize (arrows in C), while the choroidal injection creates a blurred hyper reflective rim at the leading edge of the bleb, and the retinal schisis is evident by the sharp demarcation of its leading edge (E). Both red scale bars = 200 μ m in 4B. All images 4B through 4E are scaled equally.

Figure 5: Mapping and Quantifying Outer Retinal Changes following Subretinal injection. A method was developed to identify regions of interest during follow-up examination of mice that had subretinal injection of vector, with 3D-plotting of ONL measurements from multiple OCT b-

scans. A 2HRho1T/1T animal was injected with a self-complementary adeno-associated virus expressing both GFP and the lead candidate hammerhead ribozyme (scAAV-GFP ad6 hhRz 725) (OS eye) in a toxicity screen. **(A)** Imaged immediately following, the areal extent of the injection was mapped by placing calipers at the leading edge of the bleb at the point where the outer segments separate from the RPE in the b-scans (Left panel (red caliper)). The position of the caliper tool is automatically mapped to the fundus image, and this is repeated and compiled for as many b-scans as necessary, which depend upon the desired resolution (every 5th scan in **(A)** (right panel)). Subsequent OCT studies (every 2 weeks) imaged the same region of the retina to allow superimposition; the ONH and retinal blood vessels are landmarks to facilitate the Cartesian or rotational adjustments. The entire region of the retina was measured for ONL thickness provided the required boundaries (OPL and ELM) were visible. **(B)** To map the ONL length over the injected surface the caliper positions (color coded) are again mapped onto the fundus image and compiled into a composite image. Every 5th b-scan from the OCT images was measured with built-in calipers at up to ten points across the retina. **(C)** Pre- and post-compiled images are rotated, using imaging software to align retinal vasculature, which allows data points within the detached retinal region retina to be identified by image overlay and separated. **(D)** The data set is mapped into a table format, identical to the fundus image array, and divided into two groups (measurements within the bleb (red highlights) and those that are not). **(E)** Data is presented using a 3D surface plotting feature, which allows visualization of ONL thickness over the entire imaged region. This allows assessment of quantitative differences between injected and non-injected regions of the eye. The crevice in the 3D plot **(E)** provides a convenient way to segregate the data set of ONL measurements within the region of the detached retina from the region that remained attached immediately following injection.

Table 1: Program used to pull the glass needles. Program parameters to achieve glass needles useful for subretinal by trans-scleral, transchoroidal approach.

DISCUSSION:

HR-SD-OCT provides a simple method for characterization of potential animal models of human disease to determine their usefulness in testing potential therapeutics. The ability to quickly and reliably characterize a potential animal model of human disease is critical to the process of therapeutic drug discovery (*e.g.*, replacement gene therapy, ribozyme or shRNA knockdown gene therapy, combined gene therapy). HR-SD-OCT provides a simple, quick, and non-invasive method for evaluating retinal health that can be used to characterize and monitor the progression of the retinal degeneration in almost any mouse model. The OCT images can be used to obtain measurements of any or all of the different layers of the retina, which may provide a detailed assessment of an outer retinal (photoreceptor) degeneration over time or the impact of therapeutic rescue attempts on the degeneration extent or kinetic timeline. HR-SD-OCT can also be used to assess toxicity of delivered vector or materials. The most significant impact on a photoreceptor retinal degeneration research program is the ability to make refined measurements of ONL over time in live animals. One can plot a retinal degeneration timeline to extract a time constant, which is a critical first step to evaluate the efficacy and toxicity of candidate therapeutics in the same models over a temporal window of therapeutic opportunity. This technology also allows for significant savings of precious resources (animals and time)

relative to classical endpoint histology by allowing the researcher to identify abnormalities in the animal cohort prior to entering a study and eliminating animals that do not meet experimental criteria (*e.g.*, successful subretinal delivery).

The need for precise delivery of certain therapeutics into the subretinal space of the mouse eye is challenging, and HR-SD-OCT provides an accurate visual confirmation of successful subretinal injections as a criterion for ongoing inclusion of animals in the pre-clinical study design. Extensive effort is required to frequently follow animals injected in gene therapy studies over time, since these models often simulate human retinal degenerative diseases where disease timelines emerge over decades. Numerous follow-up examinations are required to determine therapeutic efficacy or to assess toxicity. A solution to this critical challenge is to have the ability to identify and remove animals from study designs, which are surgical failures for delivery of the therapeutic vector. The ability to deliver a successful injection for a well-trained technician with years of experience has approached 90% if injecting one eye per animal, and approximately 80% success if injecting both eyes. With this efficiency level, removal from the study design of animals with unsuccessful injections is advantageous to hypothesis testing. This not only saves critical time but also allows for more consistent and predictable outcomes. Additionally, HR-SD-OCT allows one to decrease the number of animals required for any one experiment by allowing the same animals to be followed over time, which decreases the animal-to-animal variability in both experimental and control groups, and allows more robust statistical evaluation of hypotheses about the potential efficacy and toxicity of candidate therapeutics.

The extent of retinal coverage by a subretinal injection is typically not 100%, which may itself be toxic^{31,32,33,34}. Hence, the ability to distinguish between transduced and non-transduced regions is critical to proper testing of hypotheses of rescue and toxicity for a given candidate therapeutic. The creative use of available software tools allows for precise mapping of subretinal injections in the mouse eye. The immediate imaging of the injected eye provides direction for follow-up imaging to regions of interest, and the ability to compare regions which have been transduced to regions which have not been treated within the same globe. Depending on the mapping precision desired, this process can be performed for each b-scan or periodically sampling from the ensemble of b-scans collected immediately post injection and compiling all the fundus images into a single image using graphics software so that the piecewise continuous border is carefully mapped onto the fundus image. Comparing the images from immediately after injection to follow-up images requires that the images be aligned so that measurement positions can be mapped onto the fundus image, and the data points can be segregated into injection site and non-injected regions of the retina. The mapping of the optic nerve head and the retinal blood vessels can also be accomplished using this same methodology, which aids in the orientation of the eye when attempting to align the post-injection images with subsequent follow-up images. This information can be used in subsequent imaging to identify the region of the retina where the injection had occurred. Of course, when the animals are euthanized, the location of EGFP expression, delivered by an AAV vector also containing a candidate therapeutic gene (*e.g.*, ribozyme), can also be used to compare the location of transduction with the area determined by image mapping that relies on the location of blood vessels. This will allow the identification of

diffusion of vector in the subsequently closed subretinal space beyond areas of anatomic detachment.

Our success with the use of gold NPs to label the subretinal bleb was limited due to toxicity induced by the materials used. We would encourage further investigation of such materials to label the extent of subretinal blebs, if alternative preparations (varying dimensions, surface modifications) can be found that do not induce toxicity.

The HR-SD-OCT provides an enormous amount of information with significantly less time and resources, and can be quantitated to provide more information about efficacy and toxicity of potential therapeutics compared to traditional methodologies like histology. The use of this technology enables the researcher to alleviate one of the severe bottlenecks in preclinical retinal drug discovery³⁵. The mouse RIS and HR-SD-OCT are powerful tools to aid preclinical retinal gene therapy studies as a component of our RNA Drug Discovery program. These tools can be broadly applied.

ACKNOWLEDGEMENTS:

This material is based upon work supported, in part, by the Department of Veterans Affairs (VA), Veterans Health Administration, Office of Research and Development (Biomedical Laboratory Research and Development) (VA Merit Grant 1I01BX000669). JMS is employed, in part, as Staff Physician-Scientist, Ophthalmology, by VA WNY; MCB is employed, in part, by VA WNY. The study was conducted at, and supported in part by, the Veterans Administration Western New York Healthcare System (Buffalo, NY). Contents do not represent the views of the Department of Veterans Affairs or the United States Government. Also supported, in major part, by NIH/NEI R01 grant EY013433 (PI: JMS), NIH/NEI R24 grant EY016662 (UB Vision Infrastructure Center, PI: M Slaughter, Director- Biophotonics Module: JMS), an Unrestricted Grant to the Department of Ophthalmology/University at Buffalo from Research to Prevent Blindness (New York, NY), and a grant from the Oishei Foundation (Buffalo, NY). We acknowledge the gift of the hC1 transgenic *RHO*^{P347S} line and the exon 1 mouse *RHO* knockout from Dr. Janis Lem (Tufts New England Medical Center, Boston, MA), and the gift of the NHR-E transgene model in the heterozygous state on the mouse exon 2 *RHO* knockout background from Drs. G. Jane Farrar and Peter Humphries (Trinity College, Dublin, IRE).

DISCLOSURES:

Commercial Relationships: MCB: None; JMS: None. The retinal imaging system (RIS)²³ used in this study is a novel device of substantial use to any group seeking to conduct gene therapy delivery studies in mice, rodents, or small animals. While the authors have no conflicts to declare with respect to this device at this time, the University at Buffalo- SUNY and the Veterans Administration have rights in the intellectual property and may seek to commercialize this instrument in the future.

REFERENCES:

1. Regus-Leidig, H. *et al.* *In-vivo* knockdown of Piccolino disrupts presynaptic ribbon morphology in mouse photoreceptor synapses. *Front Cell Neurosci.* 8, 259, 1-13 (2014).

2. Jiang L., Frederick J.M., and Baehr W. RNA interference gene therapy in dominant retinitis pigmentosa and cone-rod dystrophy mouse models caused by GCAP1 mutations. *Front Mol Neurosci*, 7, 25: 1-8 (2014).
3. Seo, S. et al. Subretinal gene therapy of mice with Bardet-Biedl Syndrome Type-1, *Invest. Ophthalmol. Vis. Sci.* 54, (9), 6118-6132 (2013).
4. Molday, L. L. et al. RD3 gene delivery restores guanylate cyclase localization and rescues photoreceptors in the RD3 mouse model of Leber congenital amaurosis 12, *Hum. Mol. Genet*, 22 (19), 3894-3905 (2014).
5. Pang, J.J. et al. AAV-mediated gene therapy in mouse models of recessive retinal degeneration. *Curr. Mol. Med.* (3), 316-330 (2012).
6. Vandenberghe L.H., Auricchio A., Novel adeno-associated viral vectors for retinal gene therapies, *Gene Ther.* Feb; 19(2): 162-168 (2012).
7. Tenenbaum, L., Lehtonen E., Monahan, P.E. Evaluation of risks related to the use of adeno-associated virus-based vectors. *Curr. Gene Ther.* Dec; 3(6): 545-565 (2003).
8. Parikh, S., Le, A., Davenport, J., Gorin, M.B., Nusinowitz, S., Matynia, A. An alternative and validated injection method for accessing the subretinal space *via* a transcleral posterior approach. *J. Vis. Exp.* (118), e54808, doi: 10.3791/54808 (2016).
9. Bainbridge, J.W.B., Mistry, A.R., Thrasher, A.J., and Ali, R.R. Gene therapy for ocular angiogenesis, *Clinical Science*. 104: 561-575 (2003).
10. Igarashi T., Miyake K., Asakawa N., Miyake N., Shimada T., Takahashi H. Direct comparison of administration routes for AAV-8 mediated ocular gene therapy. *Curr. Eye Res.*, May; 38(5): 569-77 (2013).
11. Bennett, J., Duan, D., Engelhardt, J.F., and Maguire, A.M. Real-time noninvasive *in vivo* assessment of adeno-associated virus-mediated retinal transduction. *Invest. Ophthalmol. Vis. Sci.* 38: 2857-2863 (1997).
12. Ruggeri, M. et al. In vivo three-dimensional high-resolution imaging of the rodent retinal with spectral-domain optical coherence tomography. *Invest. Ophthalmol. Vis. Sci.* 48(4): 1808-1814 (2007).
13. Berger, A. et al. Spectral domain optical coherence tomography of the rodent eye: highlighting layers of the outer retina using signal averaging and comparison with histology. *PLoS One* 9(5): e96494 (2014).
14. Dysli, C., Enzmann, V., Sznitman, R., Zinkernagel, M.S. Quantitative analysis of mouse retinal layers using automated segmentation of spectral domain optical coherence tomography images. *TVST* 4(4): 9 (2015).
15. Bhootada, Y., Choudhury, S., Gully, C., and Gorbatyuk, M. Targeting caspase-12 to preserve vision in mice with inherited retinal degeneration. *Invest. Ophthalmol. Vis. Sci.* 56: 4725-4733 (2015).
16. Wert, K.J., Skeie, J.M., Davis, R.J., Tsang, S.H., Mahajan, V.B. Subretinal injection of gene therapy vectors and stem cells in the perinatal mouse eye. *J. Vis. Exp.* (69), e4286, doi: 10.3791/4286 (2012).
17. Berger, A, et al., Spectral-domain optical coherence tomography of the rodent eye: highlighting layers of the outer retina using signal averaging and comparison with histology. *PLoS One*, 9(5): e96494 (2014).

18. Muhlriedel, R., Michalakis, S., Garrido, M.G., Biel, M., Seeliger, M.W. Optimized technique for subretinal injections in mice. *Methods in Molecular Biology*, Clifton, NJ, doi: 10.1007/978-1-62703-080-9_24 (2013).
19. Sarra, G.M., et al. Kinetics of transgene expression in mouse retina following subretinal injection of recombinant adeno-associated virus. *Vision Res.*, 42, 541-549. (2002)
20. Yan, Q.I., et al. Trans-corneal subretinal injection in mice and its effect on the function and morphology of the retina. *PLoS One*, 10(8): e0136523 doi: 10.1371 (2015).
21. Park, S.W., Kim, J.H., Park, W.J., and Kim, J.H. Limbal approach-subretinal injection of viral vectors for gene therapy in mice retinal pigment epithelium. *J. Vis. Exp.* (102), e53030, doi: 10.3791/53030 (2015).
22. Westenskow, P.D., et al. Performing subretinal injections in rodents to deliver retinal pigment epithelium cells in suspension. *J. Vis. Exp.* (95), e52247, doi: 10.3791/52247 (2015).
23. Butler, M.C., and Sullivan, J.M. A novel, real-time, in vivo mouse retinal imaging system. *Invest. Ophthalmol. Vis. Sci.* 56(12): 7159-7168 (2015).
24. Rolling, F. et al. Evaluation of adeno-associated virus-mediated gene transfer into the rat retina by clinical fluorescence photography. *Hum. Gene Ther.* 10: 641-648 (1999).
25. Ferguson, L.R., Grover, S., Dominguez, J.M. II, Balaiya, S., Chalam, K.V. Retinal thickness measurement obtained with spectral domain optical coherence tomography assisted optical biopsy accurately correlates with *ex vivo* histology. *PLoS One* 9(10): e111203 (2014).
26. Li, T., Snyder, W.K., Olsson, J.E., and Dryja, T.P. Transgenic mice carrying the dominant rhodopsin mutation P347S: evidence for defective vectorial transport of rhodopsin to the outer segments. *Proc. Natl. Acad. Sci. USA*; 93: 14176-14181 (1996).
27. Brill, E. et al. A novel form of transducin-dependent retinal degeneration: accelerated retinal degeneration in the absence of rod transducing. *Invest. Ophthalmol. Vis. Sci.*, 48: 5445-5453 (2007).
28. Olsson, J.E. et al. Transgenic mice with a rhodopsin mutation (Pro23His): a mouse model of autosomal dominant retinitis pigmentosa. *Neuron*, 9: 815-830 (1992).
29. Humphries, M.M. et al. Retinopathy induced in mice by targeted disruption of the rhodopsin gene. *Nat. Genet.*, 15: 216-219 (1997).
30. Hruby, K. Clinical examination of the vitreous body. *Proc. Roy. Soc. Med.* 47: 163-170 (1953).
31. Kolniak, T.A. and Sullivan, J.M. Rapid, cell-based toxicity screen of potentially therapeutic post-transcriptional gene silencing agents. *Experimental Eye Research.* 92: 328-337 (2011).
32. Qi, Y. et al. Trans-corneal subretinal injection in mice and its effect on the function and morphology of the retina. *PLoS One* 10(8): e0136523 (2015).
33. Timmers, A.M., Zhang, H., Squitieri, A., and Gonzalez-Pola, C. Subretinal injections in rodent eyes: effects on electrophysiology and histology of rat retina. *Mol. Vis.* 7: 131-137 (2000).
34. Johnson, C.J., Berglin, L., Chrenek, M.A., Redmond, T.M., Boatright, J.H., Nickerson, J.M. Technical brief: subretinal injection and electroporation into adult mouse eyes. *Mol. Vis.* 14: 2211-2226 (2008).
35. Sullivan, J.M., Yau, E.H., Taggart, R.T., Butler, M.C., and Kolniak, T.A. Bottlenecks in development of therapeutic post-transcriptional gene silencing agents. *Vision Res.* 48: 453-469 (2008).

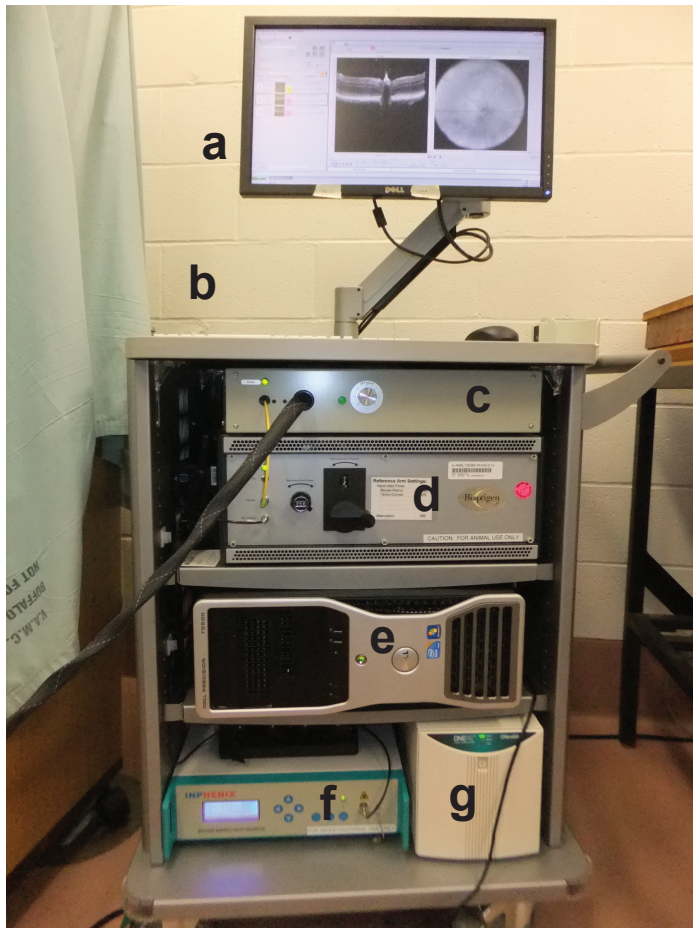
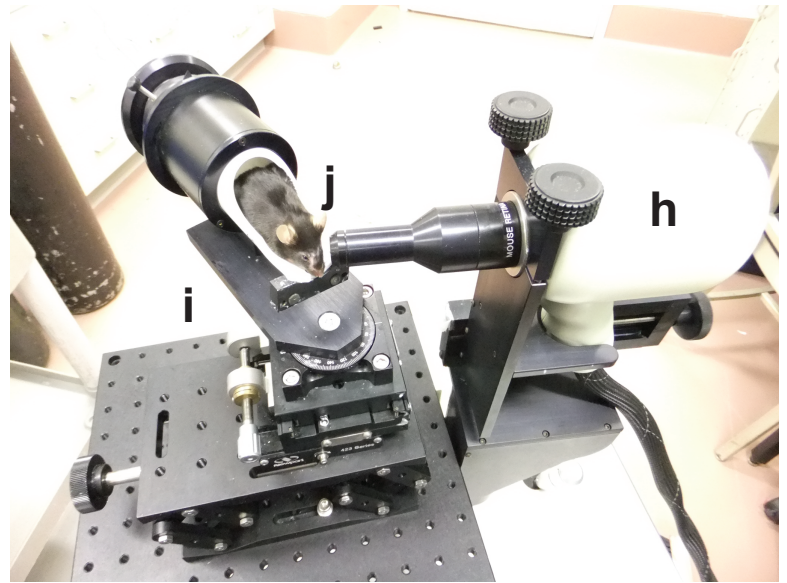
A**B**

Figure 2

C57BL/6(J) (14 weeks)

A



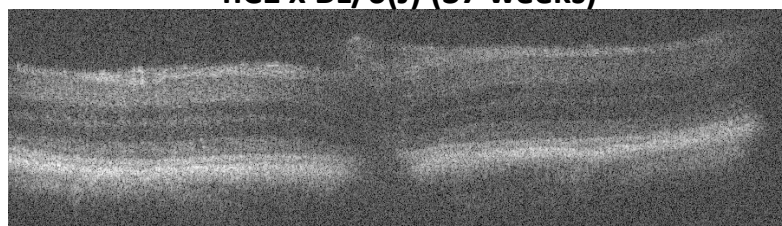
hC1 x BL/6(J) (3 weeks)



hC1 x BL/6(J) (10 weeks)



hC1 x BL/6(J) (37 weeks)



hC1/hC1//mWT/mWT (3 weeks)



B

Retinal degeneration in C1xBL6(J) mouse model over time

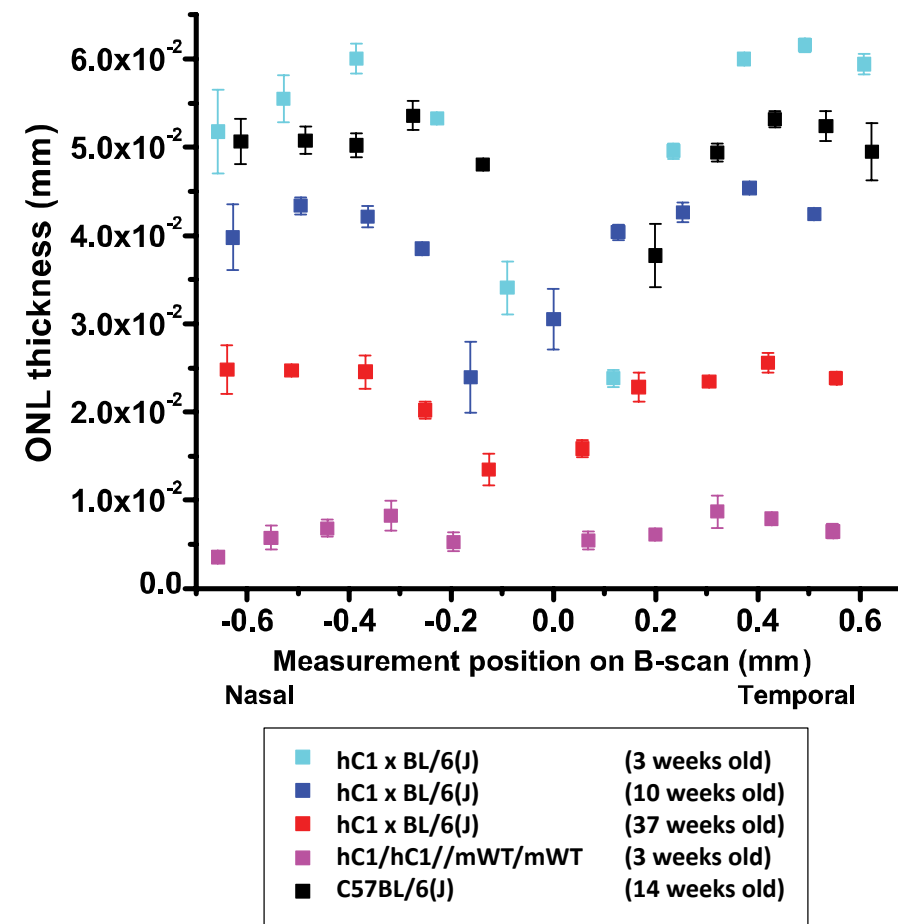
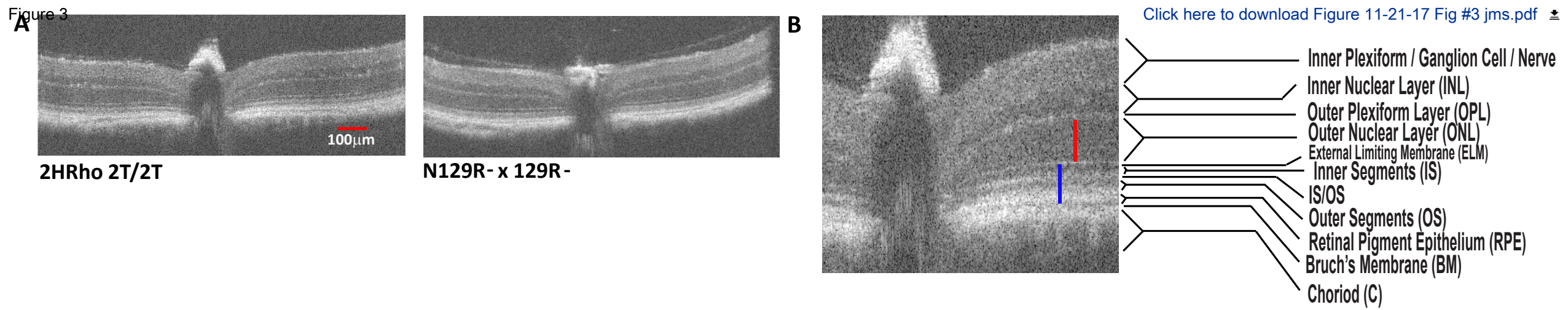


Figure 3



C

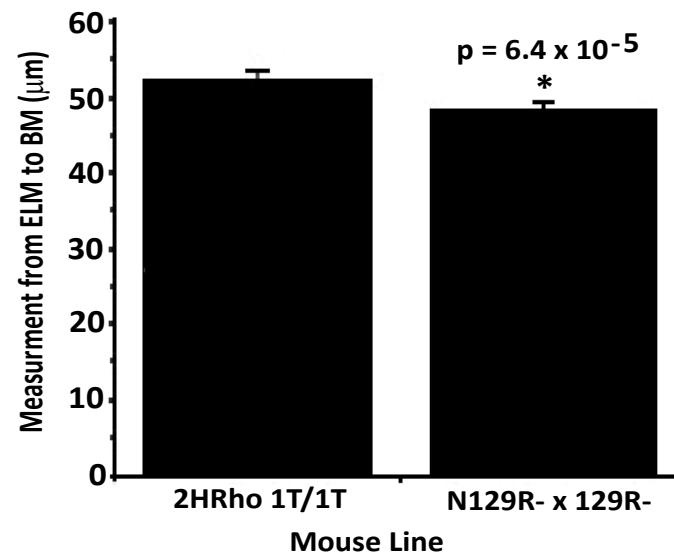
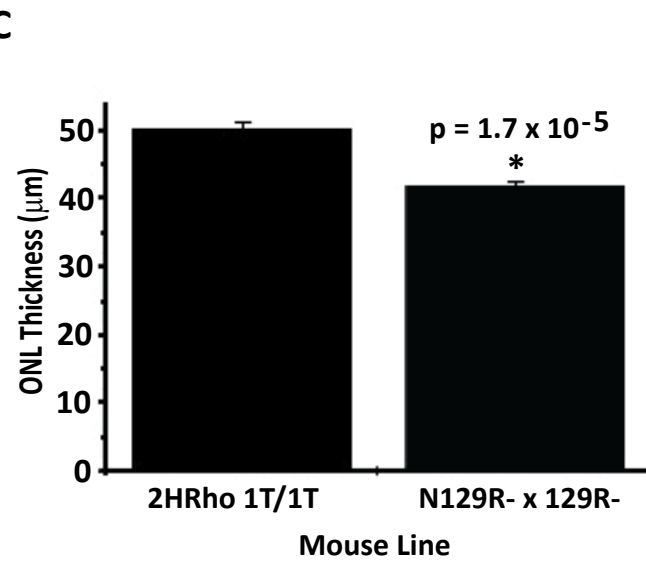


Figure 4

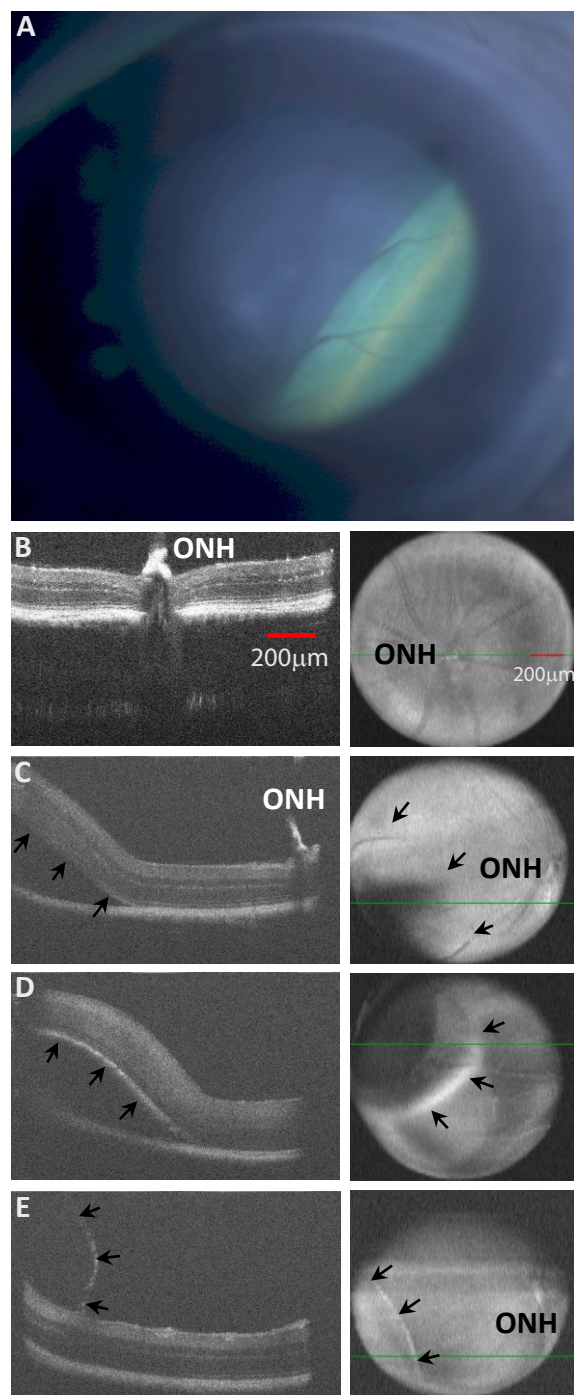


Figure 5

[Click here to download Figure 5E 11-27-17 mod.pdf](#)

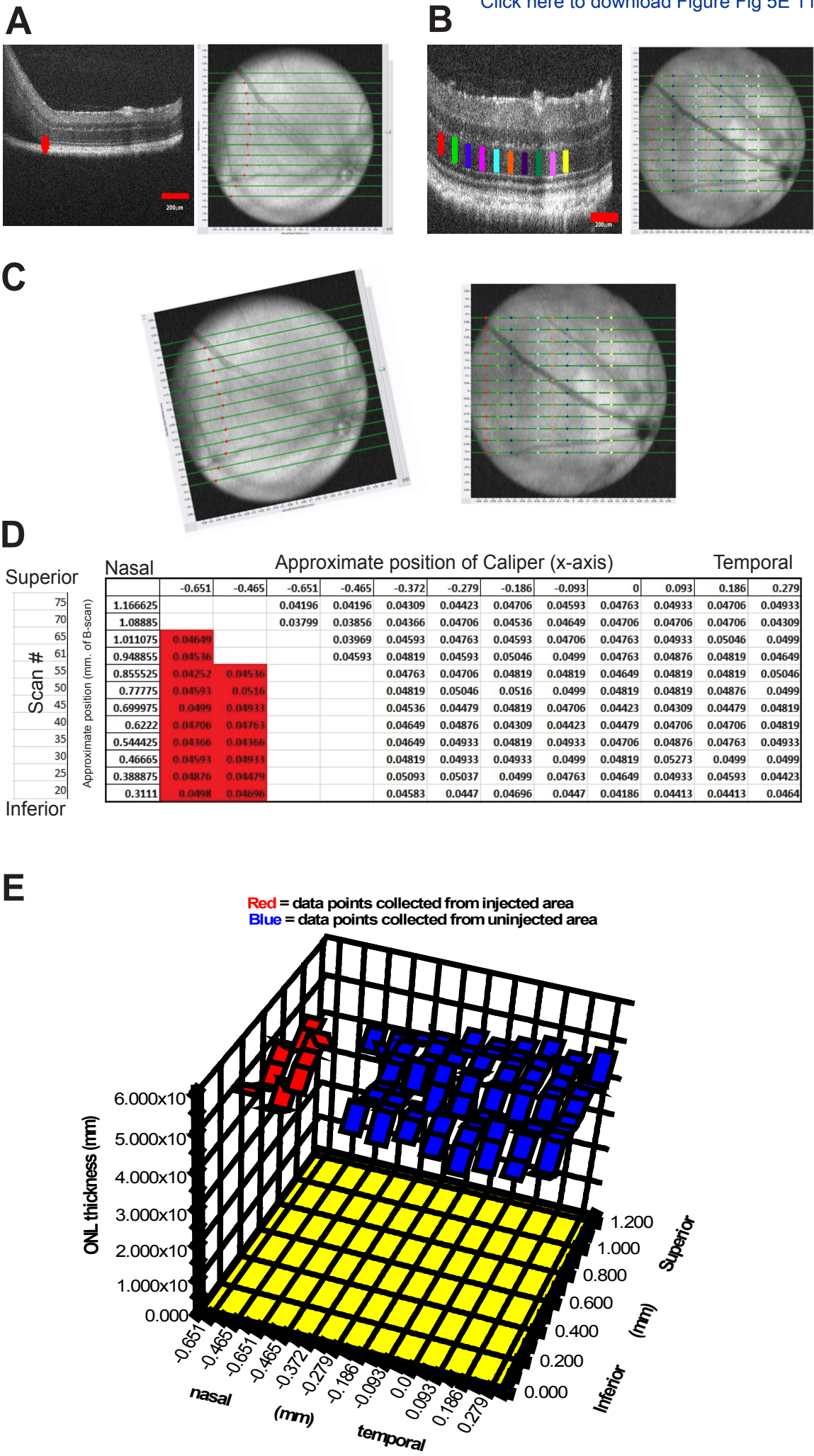


Table #1 Values used in program to pull the glass needles.					
	Heat	Pull	Velocity	Time	
Step 1	780	25	5	250	
Step 2	780	40	10	250	
Step 3	780	10	5	250	
Step 4	790	10	10	250	
Step 5	780	0	23	250	

Materials / Equipment	Company
C57BL6 (J)	Jackson Laboratories
N129R-	N/A
2HRho 1T/1T	N/A
Envisu R-2200 Ocular Coherence Tomography Instrument (OCT)	Bioptigen
Retinal Imaging System (RIS)	In-house
Stemi 2000C Microscope	Zeiss
P-97 Flaming/Brown micropipette puller	Sutter Instrument Co
MMN-33 micro manipulator	Narishige USA
PLI-100 micro injector	Harvard Apparatus
Micropipette Holder (Rotating)	In-house
Micropipette Storage Receptacle	World Precision Instruments Inc.
Borosilicate glass capillary tubes 1.5-1.8 X 100mm,	Harvard Apparatus
2,2,2-Tribromoethanol	SIGMA Aldrich
Tert-amyl Alcohol	SIGMA Aldrich
Atropine Sulfate Ophthalmic Solution, USP 1%	Akorn Inc.
Goniovisc	BioVision Limited
Cyclopentolate Hydrochloride Ophthalmic Solution, USP 2%	Akorn Inc.
Gentamicin Sulfate Ointment USP, 0.1%	Perigo
Systane Ultra	Alcon Laboratories, Inc.
Tetracaine Hydrochloride Ophthalmic Solution, USP 0.5%	Bausch and Lomb
DPBS	Gibco Life Technologies

Virus Preparations	ViGene /UNC
Gold nanorods	NANOPARTz
Fluorescein Sulfate AK-FLUOR 25%	Akorn Inc.
Coverslips	Fisher Scientific
Forceps	Milton
Needles 30 guage	Beckton Dickenson
Syringes	Beckton Dickenson
Bioptigen software Package	Bioptigen
Proparacaine Hydrochloride Ophthalmic Solution, USP 0.5%	Akorn Inc.
Windows Excel	Microsoft
Adobe Illustrator	Adobe
Scale	Mettler
Scissors	World Precision Instruments
Ear punch	Nat'l band
CL 100 Light source	Welch Allyn
Nitrogen Gas	Jackson Welding Supply
Heated Water bath	Neslab
Heating plate	In House
Heating mat	Cincinnati Sub Zero
Clay mouse holder	Plast.i.clay American Art Clay Co.
Betadine	MedLine
Cotton Tip Applicators	American Health Service
EtOH 70%	Fisher Scientific
Gloves Nitrile	VWR

Diagnosys ERG Color Dome instrument	Diagnosys Inc.
Contact lenses	In-house
Diagnosys Software	Diagnosys Inc.
Origin 6.1 software	OriginLab Corp.
Reference electrodes	Ocuscience

Catalog Number
664
N/A
N/A
90-R2200-U1-120.
N/A
000000-1106-133
p-97
MMN-33
64-1736
N/A
E210
30-0053
T48402-25G
240486-100ML
NDC 17478-215-05
NDC 17238-610-15
NDC 17478-097-10
NDC 45802-046-35
9006619-1013
NDC 24208-920-64
14190-136

N/A

D12M-850-1.75

NDC 17478-250-20

12-548-A

18-825

W11604

309659

N/A

NDC 17478-263-12

N/A

CL100

N/A

RTE-140

N/A

273

N/A

NDC53329-938-06

Ctag

BP2818-100

89038-272

D125

N/A

N/A

N/A

F-Thread Electrode (DTL) 24"



1 Alewife Center #200
Cambridge, MA 02140
tel. 617.945.9051
www.jove.com

ARTICLE AND VIDEO LICENSE AGREEMENT

Title of Article:

Ultrahigh Resolution Mouse Optical Coherence Tomography to Aid Intraocular Injection in Retinal Gene Therapy Research

Author(s):

Mark C. Butler, M.S. and Jack M. Sullivan, M.D., Ph.D.

Item 1 (check one box): The Author elects to have the Materials be made available (as described at <http://www.jove.com/author>) via: ☒ Standard Access ☐ Open Access

Item 2 (check one box):

- ☐ The Author is NOT a United States government employee.
- ☒ The Author is a United States government employee and the Materials were prepared in the course of his or her duties as a United States government employee.
- ☐ The Author is a United States government employee but the Materials were NOT prepared in the course of his or her duties as a United States government employee.

ARTICLE AND VIDEO LICENSE AGREEMENT

1. **Defined Terms.** As used in this Article and Video License Agreement, the following terms shall have the following meanings: “**Agreement**” means this Article and Video License Agreement; “**Article**” means the article specified on the last page of this Agreement, including any associated materials such as texts, figures, tables, artwork, abstracts, or summaries contained therein; “**Author**” means the author who is a signatory to this Agreement; “**Collective Work**” means a work, such as a periodical issue, anthology or encyclopedia, in which the Materials in their entirety in unmodified form, along with a number of other contributions, constituting separate and independent works in themselves, are assembled into a collective whole; “**CRC License**” means the Creative Commons Attribution-Non Commercial-No Derivs 3.0 Unported Agreement, the terms and conditions of which can be found at: <http://creativecommons.org/licenses/by-nc-nd/3.0/legalcode>; “**Derivative Work**” means a work based upon the Materials or upon the Materials and other pre-existing works, such as a translation, musical arrangement, dramatization, fictionalization, motion picture version, sound recording, art reproduction, abridgment, condensation, or any other form in which the Materials may be recast, transformed, or adapted; “**Institution**” means the institution, listed on the last page of this Agreement, by which the Author was employed at the time of the creation of the Materials; “**JoVE**” means MyJoVE Corporation, a Massachusetts corporation and the publisher of *The Journal of Visualized Experiments*; “**Materials**” means the Article and / or the Video; “**Parties**” means the Author and JoVE; “**Video**” means any video(s) made by the Author, alone or in conjunction with any other parties, or by JoVE or its affiliates or agents, individually or in collaboration with the Author or any other parties, incorporating all or any portion of the Article, and in which the Author may or may not appear.

2. **Background.** The Author, who is the author of the Article, in order to ensure the dissemination and protection of the Article, desires to have the JoVE publish the Article and create and transmit videos based on the Article. In furtherance of such goals, the Parties desire to memorialize in this Agreement the respective rights of each Party in and to the Article and the Video.

3. **Grant of Rights in Article.** In consideration of JoVE agreeing to publish the Article, the Author hereby grants to JoVE, subject to **Sections 4 and 7** below, the exclusive, royalty-free, perpetual (for the full term of copyright in the Article, including any extensions thereto) license (a) to publish, reproduce, distribute, display and store the Article in all forms, formats and media whether now known or hereafter developed (including without limitation in print, digital and electronic form) throughout the world, (b) to translate the Article into other languages, create adaptations, summaries or extracts of the Article or other Derivative Works (including, without limitation, the Video) or Collective Works based on all or any portion of the Article and exercise all of the rights set forth in (a) above in such translations, adaptations, summaries, extracts, Derivative Works or Collective Works and (c) to license others to do any or all of the above. The foregoing rights may be exercised in all media and formats, whether now known or hereafter devised, and include the right to make such modifications as are technically necessary to exercise the rights in other media and formats. If the “Open Access” box has been checked in **Item 1** above, JoVE and the Author hereby grant to the public all such rights in the Article as provided in, but subject to all limitations and requirements set forth in, the CRC License.

ARTICLE AND VIDEO LICENSE AGREEMENT

4. Retention of Rights in Article. Notwithstanding the exclusive license granted to JoVE in **Section 3** above, the Author shall, with respect to the Article, retain the non-exclusive right to use all or part of the Article for the non-commercial purpose of giving lectures, presentations or teaching classes, and to post a copy of the Article on the Institution's website or the Author's personal website, in each case provided that a link to the Article on the JoVE website is provided and notice of JoVE's copyright in the Article is included. All non-copyright intellectual property rights in and to the Article, such as patent rights, shall remain with the Author.

5. Grant of Rights in Video – Standard Access. This **Section 5** applies if the "Standard Access" box has been checked in **Item 1** above or if no box has been checked in **Item 1** above. In consideration of JoVE agreeing to produce, display or otherwise assist with the Video, the Author hereby acknowledges and agrees that, Subject to **Section 7** below, JoVE is and shall be the sole and exclusive owner of all rights of any nature, including, without limitation, all copyrights, in and to the Video. To the extent that, by law, the Author is deemed, now or at any time in the future, to have any rights of any nature in or to the Video, the Author hereby disclaims all such rights and transfers all such rights to JoVE.

6. Grant of Rights in Video – Open Access. This **Section 6** applies only if the "Open Access" box has been checked in **Item 1** above. In consideration of JoVE agreeing to produce, display or otherwise assist with the Video, the Author hereby grants to JoVE, subject to **Section 7** below, the exclusive, royalty-free, perpetual (for the full term of copyright in the Article, including any extensions thereto) license (a) to publish, reproduce, distribute, display and store the Video in all forms, formats and media whether now known or hereafter developed (including without limitation in print, digital and electronic form) throughout the world, (b) to translate the Video into other languages, create adaptations, summaries or extracts of the Video or other Derivative Works or Collective Works based on all or any portion of the Video and exercise all of the rights set forth in (a) above in such translations, adaptations, summaries, extracts, Derivative Works or Collective Works and (c) to license others to do any or all of the above. The foregoing rights may be exercised in all media and formats, whether now known or hereafter devised, and include the right to make such modifications as are technically necessary to exercise the rights in other media and formats. For any Video to which this Section 6 is applicable, JoVE and the Author hereby grant to the public all such rights in the Video as provided in, but subject to all limitations and requirements set forth in, the CRC License.

7. Government Employees. If the Author is a United States government employee and the Article was prepared in the course of his or her duties as a United States government employee, as indicated in **Item 2** above, and any of the licenses or grants granted by the Author hereunder exceed the scope of the 17 U.S.C. 403, then the rights granted hereunder shall be limited to the maximum rights permitted under such

statute. In such case, all provisions contained herein that are not in conflict with such statute shall remain in full force and effect, and all provisions contained herein that do so conflict shall be deemed to be amended so as to provide to JoVE the maximum rights permissible within such statute.

8. Likeness, Privacy, Personality. The Author hereby grants JoVE the right to use the Author's name, voice, likeness, picture, photograph, image, biography and performance in any way, commercial or otherwise, in connection with the Materials and the sale, promotion and distribution thereof. The Author hereby waives any and all rights he or she may have, relating to his or her appearance in the Video or otherwise relating to the Materials, under all applicable privacy, likeness, personality or similar laws.

9. Author Warranties. The Author represents and warrants that the Article is original, that it has not been published, that the copyright interest is owned by the Author (or, if more than one author is listed at the beginning of this Agreement, by such authors collectively) and has not been assigned, licensed, or otherwise transferred to any other party. The Author represents and warrants that the author(s) listed at the top of this Agreement are the only authors of the Materials. If more than one author is listed at the top of this Agreement and if any such author has not entered into a separate Article and Video License Agreement with JoVE relating to the Materials, the Author represents and warrants that the Author has been authorized by each of the other such authors to execute this Agreement on his or her behalf and to bind him or her with respect to the terms of this Agreement as if each of them had been a party hereto as an Author. The Author warrants that the use, reproduction, distribution, public or private performance or display, and/or modification of all or any portion of the Materials does not and will not violate, infringe and/or misappropriate the patent, trademark, intellectual property or other rights of any third party. The Author represents and warrants that it has and will continue to comply with all government, institutional and other regulations, including, without limitation all institutional, laboratory, hospital, ethical, human and animal treatment, privacy, and all other rules, regulations, laws, procedures or guidelines, applicable to the Materials, and that all research involving human and animal subjects has been approved by the Author's relevant institutional review board.

10. JoVE Discretion. If the Author requests the assistance of JoVE in producing the Video in the Author's facility, the Author shall ensure that the presence of JoVE employees, agents or independent contractors is in accordance with the relevant regulations of the Author's institution. If more than one author is listed at the beginning of this Agreement, JoVE may, in its sole discretion, elect not take any action with respect to the Article until such time as it has received complete, executed Article and Video License Agreements from each such author. JoVE reserves the right, in its absolute and sole discretion and without giving any reason therefore, to accept or decline any work submitted to JoVE. JoVE and its employees, agents and independent contractors shall have

ARTICLE AND VIDEO LICENSE AGREEMENT

full, unfettered access to the facilities of the Author or of the Author's institution as necessary to make the Video, whether actually published or not. JoVE has sole discretion as to the method of making and publishing the Materials, including, without limitation, to all decisions regarding editing, lighting, filming, timing of publication, if any, length, quality, content and the like.

11. **Indemnification.** The Author agrees to indemnify JoVE and/or its successors and assigns from and against any and all claims, costs, and expenses, including attorney's fees, arising out of any breach of any warranty or other representations contained herein. The Author further agrees to indemnify and hold harmless JoVE from and against any and all claims, costs, and expenses, including attorney's fees, resulting from the breach by the Author of any representation or warranty contained herein or from allegations or instances of violation of intellectual property rights, damage to the Author's or the Author's institution's facilities, fraud, libel, defamation, research, equipment, experiments, property damage, personal injury, violations of institutional, laboratory, hospital, ethical, human and animal treatment, privacy or other rules, regulations, laws, procedures or guidelines, liabilities and other losses or damages related in any way to the submission of work to JoVE, making of videos by JoVE, or publication in JoVE or elsewhere by JoVE. The Author shall be responsible for, and shall hold JoVE harmless from, damages caused by lack of sterilization, lack of cleanliness or by contamination due to the making of a video by JoVE its employees, agents or independent contractors. All sterilization, cleanliness or decontamination procedures shall be solely the responsibility of the Author and shall be undertaken at the Author's

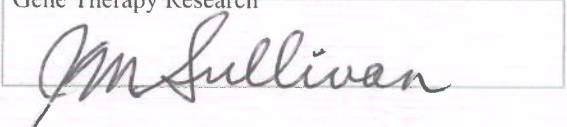
expense. All indemnifications provided herein shall include JoVE's attorney's fees and costs related to said losses or damages. Such indemnification and holding harmless shall include such losses or damages incurred by, or in connection with, acts or omissions of JoVE, its employees, agents or independent contractors.

12. **Fees.** To cover the cost incurred for publication, JoVE must receive payment before production and publication the Materials. Payment is due in 21 days of invoice. Should the Materials not be published due to an editorial or production decision, these funds will be returned to the Author. Withdrawal by the Author of any submitted Materials after final peer review approval will result in a US\$1,200 fee to cover pre-production expenses incurred by JoVE. If payment is not received by the completion of filming, production and publication of the Materials will be suspended until payment is received.

13. **Transfer, Governing Law.** This Agreement may be assigned by JoVE and shall inure to the benefits of any of JoVE's successors and assignees. This Agreement shall be governed and construed by the internal laws of the Commonwealth of Massachusetts without giving effect to any conflict of law provision thereunder. This Agreement may be executed in counterparts, each of which shall be deemed an original, but all of which together shall be deemed to me one and the same agreement. A signed copy of this Agreement delivered by facsimile, e-mail or other means of electronic transmission shall be deemed to have the same legal effect as delivery of an original signed copy of this Agreement.

A signed copy of this document must be sent with all new submissions. Only one Agreement required per submission.

CORRESPONDING AUTHOR:

Name: Jack M. Sullivan, M.D., Ph.D.
Department: Ophthalmology
Institution: University at Buffalo- SUNY; Veterans Administration Western NY Healthcare System
Article Title: Ultrahigh resolution Mouse Optical Coherence Tomography to Aid Intraocular Injection in Retinal Gene Therapy Research
Signature:  Date: 9/19/2017

Please submit a signed and dated copy of this license by one of the following three methods:

- 1) Upload a scanned copy of the document as a pdf on the JoVE submission site;
- 2) Fax the document to +1.866.381.2236;
- 3) Mail the document to JoVE / Attn: JoVE Editorial / 1 Alewife Center #200 / Cambridge, MA 02139

For questions, please email submissions@jove.com or call +1.617.945.9051

University at Buffalo- SUNY

Laboratory of Retinal and Macular Degenerations
VA West NY Healthcare System, Medical Res. Rm 238
3495 Bailey Ave.
Buffalo, N.Y. 14215



Jack M. Sullivan, M.D., Ph.D.

Director and Principal Investigator
(716) 862-6533
(716) 862-6526 FAX
js354@buffalo.edu
<http://www.smbs.buffalo.edu/ophthalmology/people.shtml>

University at Buffalo. The Ira G. Ross Eye Institute VA Western New York Healthcare System

Dr. Vineeta Bajaj, Ph.D.

Senior Scientific Editor, *Journal of Visualized Experiments*

November 22, 2017

Dear Dr. Bajaj,

We are resubmitting the revised manuscript titled: “**Ultrahigh Resolution Mouse Optical Coherence Tomography to Aid Intraocular Injection in Retinal Gene Therapy Research**” for publication in *Journal of Visualized Experiments* (JoVE). The current identifier for the manuscript is: **JoVE55894R1**.

We would like to thank the editor and the reviewers for their careful review of our manuscript, and extensive responses provided. We appreciate the opportunity to make the necessary changes to our manuscript where deficiencies existed, allowing us to provide a better manuscript for publication. We believe that we have addressed all of the concerns of the editor and the two reviewers (which are detailed below with our responses). We would appreciate a rapid review of our revised manuscript.

Response to the Editorial comments

Editorial comments:

1. The ALA says that the article will be published as standard access, however, in the editorial manager, this manuscript is marked for open access. Please check and upload new ALA if needed.

We kept it as standard submission, so adjusted in the Editorial Manager, and the ALA letter is then correct.

2. Please upload better quality figures with focused images of uniform size and resolution (at least 300dpi).

All Figures in Figures 2, 3, 4, and 5 were again uploaded from the OCT machine as high resolution TIF files (> 300 dpi) and then imported into Adobe Illustrator for processing and notations. The appearance of the images is significantly improved.

3. Please mark scale bars in all the figures with the microscope and describe it in the figure legend.

Scale bars have been added where appropriate in all retinal imaging Figures and their legends.

4. Please answer all the specific comments marked in manuscript.

A response to each critique box in the MS (.DOC) file was made. Some text added was left in red font.

5. After all formatting, please ensure that the highlight remains 2.75 pages or less (hard cut limit) of the Protocol (including headings and spacing) that identifies the essential steps of the protocol for the video, i.e., the steps that should be visualized to tell the most cohesive story of the Protocol. Presently it is 3 pages.

The highlighted component is now 2.75 pages or less (without the notations). Critical parts of the protocol for video were maintained and others were left unhighlighted (e.g. preparing the animal).

We are looking to enhance Fig. 5E for better presentation of the 3D figure. We will send this to you as soon as we have it.

We have reason to believe that a strong conflict of interest exists for Albert S. Lewin, Ph.D. and William W. Hauswirth, Ph.D. (University of Florida at Gainesville) and G. Jane Farrar, Ph.D. and Peter Humphries, Ph.D. (Trinity College, Dublin) to be reviewers of this manuscript, and we respectfully request that they be **excluded** from all aspects of the review process. There are many scientists with the expertise to conduct a merit-based peer review our manuscript. We suggest the following reviewers: Eric A. Pierce, M.D., Ph.D. (Massachusetts Eye and Ear Infirmary, Harvard Medical School), Stephen H. Tsang, M.D., Ph.D. (Columbia Univ.), Shiming Chen, Ph.D. (Washington University), Deborah Farber, Ph.D. (Jules Stein, UCLA), and Tiansen Li, M.D. Ph.D. (National Eye Institute). Contact information for these investigators is listed below. These investigators are actively working in the field of molecular biology of retinal degenerations. We have not had prior collaborations with these investigators.

As the corresponding author it is important to disclose that I am an author of a patent on development and use of post-transcriptional gene silencing agents (US: 8,252,527). There is no licensing or other financial stream from this intellectual property at this time.

We need to have this article in press by no later than 12/31/2017.

If there are any questions please do not hesitate to call upon me.

Sincerely,



Jack M. Sullivan, M.D., Ph.D.
Professor of Ophthalmology, University at Buffalo
Staff Physician Scientist, Veterans Administration Western New York Healthcare System

Corresponding Author Contact Information:

Jack M. Sullivan, M.D., Ph.D.

Professor of Ophthalmology, Adjunct in Pharmacology, Neuroscience, and Physiology/Biophysics
University at Buffalo- SUNY, The Ira G. Ross Eye Institute
Veterans Administration Western New York Healthcare System
Medical Research, Building 20, Rm 245
3495 Bailey Ave.
Buffalo, NY. 14215

(716)-862-6533 (office)

(716)-862-6526 (FAX)

jackmsullivanmdphd@yahoo.com (preferred email contact)

js354@buffalo.edu

Potential Reviewers

Eric A. Pierce, M.D., Ph.D.

Solman and Libe Friedman Associate Professor of Ophthalmology

Director, Ocular Genomics Institute

Director, Berman-Gund Laboratory for the Study of Retinal Degenerations, Mass. Eye and Ear

Director, Inherited Retinal Disorders Service, Mass. Eye and Ear Infirmary

Senior Scientist, Mass. Eye and Ear Infirmary

243 Charles Street

Boston, MA 02114

Phone: 617-573-3621

Fax: 617-573-3661

eric_pierce@meei.harvard.edu

Stephen H. Tsang, M.D., Ph.D.

Associate Professor of Ophthalmology, Pathology and Cell Biology

Columbia University School of Medicine

Edward S. Harkness Eye Institute

160 Fort Washington Avenue,

Room 513

New York, NY

(212)-342-1189

sht2@cumc.columbia.edu

Gene.targeting@gmail.com

Shiming Chen, Ph.D.

Ophthalmology and Visual Sciences

Washington University School of Medicine

660 South Euclid Ave.

St. Louis, MO 63110

USA

(314)-747-4350

(314)-747-4211 (FAX)

chen@vision.wustl.edu

Debora Farber, Ph.D.

Jules Stein Eye Institute

CHS/UCLA

100 Stein Plaza

Los Angeles, CA 90095-7000

USA

(310)-206-7375

(310)-794-7905 (FAX)

farber@jsei.ucla.edu

Tiansen Li, M.D. Ph.D.
Senior Investigator
Retinal Cell Biology and Degeneration
Intramural Program
National Eye Institute
Building 6, Room 337
6 Center Drive
Bethesda, MD 20892
(301)-443-2833
Tiansen.li@nih.gov